

# Experiment-driven Characterization of Full-Duplex Wireless Systems

Melissa Duarte, Chris Dick and Ashutosh Sabharwal

## Abstract

We present an experiment-based characterization of passive and active self-interference cancellation mechanisms and we analyze the performance of full-duplex wireless communication systems. In particular, we consider passive suppression due to antenna separation at the same node, and active cancellation in analog or digital domain. First, we show that the average amount of cancellation increases for active cancellation techniques as the received self-interference power increases. Our characterization of the average cancellation as a function of the self-interference power allows us to show that for a constant signal-to-interference ratio at the receiver antenna (before any active cancellation is applied), the rate of a full-duplex link increases as the self-interference power increases. Second, we show that applying digital cancellation after analog cancellation can sometimes increase the self-interference, and thus digital cancellation is more effective when applied selectively based on measured suppression values. Third, we complete our study of the impact of self-interference cancellation mechanisms by characterizing the probability distribution of the self-interference channel before and after cancellation.

## I. INTRODUCTION

Current deployed wireless communication systems employ either a time-division or frequency-division approach to bidirectional communication. This requires dividing the temporal and/or spectral resources into orthogonal resources and results in half-duplex wireless communication systems. The key deterrent in implementing a full-duplex wireless communication system, which

This work was partially supported by NSF Grants CNS-0551692, CNS-0923479 and CNS-1012921. The first author was also supported by a Xilinx Fellowship and a Roberto Rocca Fellowship.

M. Duarte and A. Sabharwal are with the Department of Electrical and Computer Engineering, Rice University, Houston, TX, 77005 USA, e-mail: {mduarte, ashu}@rice.edu.

C. Dick is with Xilinx Inc., San Jose, CA, 95124 USA, e-mail: chris.dick@xilinx.com.

consist on same band simultaneous bidirectional communication, is the large self-interference from a node's own transmissions in comparison to the signal-of-interest from the distant transmitting antenna. The large self-interference spans most of the dynamic range of the analog-to-digital converter in the receiving chain, which in turn dramatically increases the quantization noise for the signal-of-interest. However, recent experimental results for indoor scenarios have shown that it is possible to implement self-interference cancellation mechanisms that can sufficiently attenuate the self-interference such that the resulting full-duplex wireless system can achieve higher rates than a half-duplex system [1, 2]. Hence, recent results have demonstrated that full-duplex systems are a feasible option for future short to medium-distance wireless communications.

In this paper, we perform a data-driven analysis of the full-duplex architecture proposed in [2]. Based on extensive experimental data, our main contribution consists in characterizing the impact of different self-interference cancellation mechanisms on the performance of full-duplex wireless communication systems. We consider three methods to reduce self-interference, which can be classified as either *passive* or *active*. The passive suppression is simply attenuation caused by path-loss made possible by *antenna separation* between the transmitting antenna and the receiving antenna on the same node. To reduce the dynamic range of the self-interference, we use the active *analog cancellation* proposed in [2] where an additional RF chain is used to cancel the self-interference at the receiving antenna, before the analog-to-digital converter. In addition, we also study active *digital cancellation*, where the self-interference is removed in baseband after analog to digital conversion.

Our results show that the average amount of self-interference cancelled by active cancellation increases as the power of the self-interference signal increases. The result is intuitive because the cancelers relies on estimating the self-interference channel, and a higher self-interference power implies lower channel estimation error and hence better cancellation. Related work on implementation of self-interference cancellation mechanisms [1–4] has reported measured values of the amount of cancellation that can be achieved but a characterization of the average amount of cancellation as a function of the self-interference power has not been reported before. Our characterization of active cancellation as a function of the self-interference power allows us to show that for a constant Signal to Interference Ratio (SIR) at the receiver antenna (this is the SIR before active cancellation), the rate of a full-duplex link increases as the self-interference power increases. This appears counter-intuitive at first but follows from the fact that the average amount

of self-interference cancellation increases with increasing self-interference power. Finally, our results lead to a design rule for full-duplex systems which specifies that for two nodes that are communicating in full-duplex mode, increasing the transmission power at both nodes by the same amount increases the achievable sum rate of the full-duplex system.

Related work in [1, 2] has shown that digital cancellation, while by itself insufficient to deal with self-interference, can increase the total amount of cancellation by 5 to 10 dB when applied after analog cancellation. However, intuitively it is clear that in an ideal scenario where analog cancellation could achieve infinite dB of cancellation then having digital cancellation after analog cancellation would be unnecessary. This leads to the natural question regarding when is digital cancellation useful. We present results that show that the self-interference suppression achieved by digital cancellation when applied after analog cancellation decreases as the self-interference suppression achieved by analog cancellation increases. Further, our results show that when analog cancellation achieves large suppression then applying digital cancellation after analog cancellation can increase the noise in the system. Our results also show that digital cancellation is an excellent safety net for the cases when analog cancellation delivers poor suppression. Using these experiment-based data and results, we propose a design rule for full-duplex systems that specifies that digital cancellation is most useful when applied selectively frame-by-frame based on measured suppression performance.

We complete our study of the impact of self interference cancellation mechanisms by characterizing the distribution of the self-interference channel before and after active cancellation. Before applying active cancellation the self-interference channel is the channel between two antennas that are close to each other, consequently there is a strong Line-Of-Sight (LOS) component and the magnitude of the self-interference channel can be modeled as a Ricean distribution with large  $K$ -factor. After applying active cancellation the strong LOS component is reduced, hence, the magnitude of the self-interference channel can be modeled as a Ricean distribution with smaller  $K$ -factor [5]. We present a characterization of the  $K$ -factor values before and after active cancellation, such characterization has not been reported before.

The rest of the paper is organized as follows. In Section II-B we derive input-output equations that model the full-duplex systems we have implemented. These equations serve as a theoretical framework that we will use for explanation of our results. A description of the experiment setup is presented in Section III. In Section IV we present a characterization of the amount of

cancellation achieved by active self-interference cancellation. In Section IV we also present a characterization of the  $K$ -factor of the self-interference channel before and after cancellation. In Section V we present an analysis of the achievable rate performance of full-duplex systems. Conclusions are presented in Section VI.

## II. CHANNEL MODEL FOR TWO-WAY FULL-DUPLEX CHANNEL

In this paper, we will focus on full-duplex two-way communication, where two nodes have data for each other, and transmit and receive simultaneously in the same frequency band. We first describe the key elements of the hardware architecture, and then channel models with different stages of passive and active suppression.

### A. Hardware Architecture

Fig. 1 shows the block diagram for the narrowband full-duplex system implemented on the WARP platform [6]. The narrowband full-duplex system is implemented using the following major blocks: Upsampling and Pulse Shaping (UPS), Matched Filter and Downsampling (MFD), Digital to Analog Converters (DACs), Analog to Digital Converters (ADCs), and transmitter and receiver radios. The transmit radios upconvert the input signal from Baseband (BB) to Radio Frequency (RF) and the receive radios downconvert from RF to BB.

An additional upconverting RF chain is used for analog cancellation [2], which transmits a signal over a wire, labeled  $c_{\text{RF},i}(t)$  for Node  $i$ , to cancel the over-the-air self-interference signal at the receiving antenna *before* this signal reaches the ADC. Thus, each node uses two upconverting radio chains and one downconverting radio chain. The additional upconverting chain used for analog cancellation does not require the power amplifier since the signals used for analog cancellation,  $c_{\text{RF},1}(t)$  and  $c_{\text{RF},2}(t)$ , are being transmitted over a wire, and thus the total hardware and power requirements of the hardware architecture are less than a half duplex 2x1 Multiple Input Single Output (MISO) wireless system [2].

### B. Channel Model With Antenna Separation (No Active Cancellation)

In Fig. 1, the signal  $x_1[n, f]$  denotes the  $n$ -th symbol transmitted from Node 1 during frame  $f$  and similarly,  $x_2[n, f]$  denotes the  $n$ -th symbol transmitted from Node 2 during frame  $f$ . A frame consists of  $N_{\text{sym}}$  consecutive transmitted symbols. We define  $x_1[n, f] = \sqrt{E_{S,1}}s_1[n, f]$  and

$x_2[n, f] = \sqrt{E_{S,2}}s_2[n, f]$  where  $s_1[n, f]$  and  $s_2[n, f]$  are the constellation symbols normalized to unit energy, and  $E_{S,1}$  and  $E_{S,2}$  denote the average symbol energy. Consequently  $E[|s_1[n, f]|^2] = 1$ ,  $E[|s_2[n, f]|^2] = 1$ ,  $E[|x_1[n, f]|^2] = E_{S,1}$ , and  $E[|x_2[n, f]|^2] = E_{S,2}$ .

We use  $h_{I,1}[f]$  and  $h_{I,2}[f]$  to denote the wireless self-interference channel at Node 1 and Node 2 respectively. Similarly,  $h_{S,1}[f]$  denotes the wireless channel from Node 1 antenna  $a$  (transmit antenna) to Node 2 antenna  $A$  (receive antenna) and we use  $h_{S,2}[f]$  to denote the wireless channel from Node 2 antenna  $B$  (transmit antenna) to Node 1 antenna  $b$  (receive antenna).

We model wireless channels  $h_{S,1}[f]$ ,  $h_{S,2}[f]$ ,  $h_{I,1}[f]$ , and  $h_{I,2}[f]$  as random variables that remain constant during the transmission of a frame  $f$  and change from one frame to the next. We define  $\Omega_{S,1} = E[|h_{S,1}[f]|^2]$ ,  $\Omega_{S,2} = E[|h_{S,2}[f]|^2]$ ,  $\Omega_{I,1} = E[|h_{I,1}[f]|^2]$ , and  $\Omega_{I,2} = E[|h_{I,2}[f]|^2]$ . The distribution of channels  $h_{S,1}[f]$ ,  $h_{S,2}[f]$ ,  $h_{I,1}[f]$ , and  $h_{I,2}[f]$  will be discussed in Section IV-B.

Antenna separation is the simplest passive self-interference suppression mechanism and the amount of cancellation achieved by antenna separation depends on the propagation loss of the signal traveling through wireless channel  $h_{I,1}[f]$ . At Node 1 the received self-interference signal after antenna separation is equal to  $h_{I,1}[f]x_{RF,1}(t)$  and the received signal of interest is equal to  $h_{S,2}[f]x_{RF,2}(t)$ . Hence, the signal received at Node 1 receive antenna  $b$  is equal to  $h_{I,1}[f]x_{RF,1}(t) + h_{S,2}[f]x_{RF,2}(t)$ .

Next, we derive equations with two active self-interference suppression methods (a) active *analog cancellation* and (b) active *digital cancellation* in baseband. Since we are analyzing a symmetric two-way channel, we will focus on describing the signals at Node 1; Node 2 signals can be derived analogously. We note that since our processing is in both analog and digital domain, we will need more notation than usual to represent signals in both domains.

### C. With Analog Cancellation

To implement the analog self-interference cancellation depicted in Fig. 1, an RF adder (implemented using RF combiners) is used with one input as the signal at the receiver antenna and the other input being a signal generated at the same node and connected to the adder via a wire. At Node 1, this local signal is equal to  $h_{Z,1}[f]c_{RF,1}(t) = -h_{Z,1}[f]\hat{\kappa}_{AC,1}[f]x_{RF,1}(t)$ , where  $h_{Z,1}[f]$  denotes the magnitude and phase change that affects signal  $c_{RF,1}(t)$  when passing through a wire to the RF adder. Analog self-interference cancellation uses  $\hat{\kappa}_{AC,1}[f]$  such that  $h_{I,1}[f]x_{RF,1}(t) - h_{Z,1}[f]\hat{\kappa}_{AC,1}[f]x_{RF,1}(t) = 0$ . One can easily see that if  $\hat{\kappa}_{AC,1}[f] = h_{I,1}[f]/h_{Z,1}[f]$

then the self-interference at the input of Node 1's receiver radio will be completely cancelled. However, Node 1 will not have a perfect estimate of channels  $h_{I,1}[f]$  and  $h_{Z,1}[f]$  due to additive noise and other distortions in the system. We define the noiseless cancellation coefficient used for analog self-interference cancellation during frame  $f$  at Node 1 as  $\kappa_{AC,1}[f] = h_{I,1}[f]/h_{Z,1}[f]$  and we use  $\hat{\kappa}_{AC,1}[f]$  to denote the noisy estimate of  $\kappa_{AC,1}[f]$ . The received signal obtained after applying analog cancellation is equal to

$$y_{AC,1}[n, f] = h_{S,2}[f]x_2[n, f] + (h_{I,1}[f] - h_{Z,1}[f]\hat{\kappa}_{AC,1}[f])x_1[n, f] + w_1[n, f], \quad (1)$$

where  $w_1[n, f]$  represents the white Gaussian noise added at Node 1's receiver. If digital cancellation (described below in Section II-D) is not being used then  $\hat{\kappa}_{DC,1}[f] = \hat{\kappa}_{DC,2}[f] = 0$  (variables introduced in Section II-D) and the received signal  $y_1[n, f]$  is equal to  $y_{AC,1}[n, f]$ .

We note that any gains applied by the radios are included in the energy terms  $E_{S,1}$  and  $E_{S,1}$ , and the cancellation coefficients  $\hat{\kappa}_{AC,1}[f]$  and  $\hat{\kappa}_{AC,2}[f]$ . This reduces the amount of notation required to present the input-output equations.

#### D. With Analog and Digital Cancellation

Digital cancellation at Node 1 is simply adding  $-\hat{\kappa}_{DC,1}[f]x_1[n, f]$  in baseband to the received signal. Since digital cancellation without analog cancellation does not yield an interesting system [1, 2] (else full-duplex would not be a challenge), we will not consider the case of digital cancellation without analog cancellation. From (1) we observe that the received self-interference signal after analog cancellation is equal to  $(h_{I,1}[f] - h_{Z,1}[f]\hat{\kappa}_{AC,1}[f])x_1[n, f]$ . We define  $\tilde{h}_{AC,1}[f] = h_{I,1}[f] - h_{Z,1}[f]\hat{\kappa}_{AC,1}[f]$ . Perfect digital cancellation of the self-interference signal at Node 1 can be achieved by setting  $\hat{\kappa}_{DC,1}[f] = \tilde{h}_{AC,1}[f]$ , however, Node 1 will not have a perfect estimate of  $\tilde{h}_{AC,1}[f]$  due to noise and other distortions present in the system. We define the noiseless cancellation coefficient used for digital self-interference cancellation at Node 1 as  $\kappa_{DC,1}[f] = \tilde{h}_{AC,1}[f]$  and we use  $\hat{\kappa}_{DC,1}[f]$  to denote the noisy estimate of  $\kappa_{DC,1}[f]$ . The received signal obtained after analog and digital cancellation is equal to

$$y_{ACDC,1}[n, f] = h_{S,2}[f]x_{S,2}[n, f] + (\tilde{h}_{AC,1}[f] - \hat{\kappa}_{DC,1}[f])x_1[n, f] + w_1[n, f]. \quad (2)$$

Hence, when both analog and digital cancellation are applied the received signal  $y_1[n, f]$  is equal to  $y_{ACDC,1}[n, f]$ .

### E. Model Simplification and Summary of Model Parameters

We now rewrite (1) and (2) in terms of the average amount of cancellation achieved by different self-interference cancellation mechanisms and in terms of the normalized self-interference channel after cancellation. This will allow us to simplify the notation in our input-output equations.

We define the average amount of cancellation achieved by a self-interference cancellation mechanism as the ratio of the self-interference energy before cancellation to the self-interference energy after cancellation. Hence, the average amount of cancellation achieved by analog cancellation at Node  $i$ ,  $\alpha_{AC,i}$ , is given by

$$\alpha_{AC,i} = \frac{E \left[ |h_{I,i}[f] x_i[n, f]|^2 \right]}{E \left[ |(h_{I,i}[f] - h_{Z,i}[f] \hat{\kappa}_{AC,i}[f]) x_i[n, f]|^2 \right]} = \frac{\Omega_{I,i}}{E \left[ |h_{I,i}[f] - h_{Z,i}[f] \hat{\kappa}_{AC,i}[f]|^2 \right]} \quad (3)$$

and the average amount of cancellation achieved by combined analog and digital cancellation at Node  $i$ ,  $\alpha_{ACDC,i}$  is given by

$$\alpha_{ACDC,i} = \frac{E \left[ |h_{I,i}[f] x_i[n, f]|^2 \right]}{E \left[ |(\tilde{h}_{ASDC,i}[f] - \hat{h}_{ACDC,i}[f]) x_i[n, f]|^2 \right]} = \frac{\Omega_{I,i}}{E \left[ |\tilde{h}_{ACDC,i}[f] - \hat{h}_{ACDC,i}[f]|^2 \right]} \quad (4)$$

Further, we define the self-interference channel after cancellation as the coefficient that multiplies the self-interference signal after applying self-interference cancellation. From (1) we have that the self-interference channel after analog cancellation at Node 1 is equal to  $h_{I,1}[f] - h_{Z,1}[f] \hat{\kappa}_{AC,1}[f]$ . From (2) we have that the self-interference channel after analog and digital cancellation at Node 1 is equal to  $\tilde{h}_{AC,1}[f] - \hat{\kappa}_{DC,1}[f]$ . We define the normalized self-interference channel after analog cancellation at Node  $i$  as  $h_{AC,i}[f]$  and the normalized self-interference channel after analog and digital cancellation at Node  $i$  as  $h_{ACDC,i}[f]$ .  $h_{AC,i}[f]$  is given by

$$h_{AC,i}[f] = \frac{h_{I,i}[f] - h_{Z,i}[f] \hat{\kappa}_{AC,i}[f]}{\sqrt{E \left[ |h_{I,i}[f] - h_{Z,i}[f] \hat{\kappa}_{AC,i}[f]|^2 \right]}} \quad (5)$$

and  $h_{ACDC,i}[f]$  is given by

$$h_{ACDC,i}[f] = \frac{\tilde{h}_{AC,i}[f] - \hat{\kappa}_{DC,i}[f]}{\sqrt{E \left[ |\tilde{h}_{AC,i}[f] - \hat{\kappa}_{DC,i}[f]|^2 \right]}} \quad (6)$$

We rewrite (1) and (2) in terms of  $\alpha_{AC,1}$ ,  $\alpha_{ACDC,1}$ ,  $h_{AC,1}[f]$ , and  $h_{ACDC,1}[f]$  as follows. For a full-duplex system with active self-interference cancellation mechanism  $\Phi$  the received signal at

Node 1 is given by

$$y_{\Phi,1}[n, f] = h_{S,2}[f]x_2[n, f] + h_{\Phi,1}[f]\sqrt{\Omega_{I,1}/\alpha_{\Phi,1}}x_1[n, f] + w_1[n, f], \quad (7)$$

where  $\Phi \in \{\text{AC}, \text{ACDC}\}$ ; recall we use AC to denote Analog Cancellation and ACDC to denote Analog and Digital Cancellation.

The average received SINR per symbol at Node 1 can be computed from (7) and is given by

$$\text{SINR}_{\Phi,1} = \frac{E \left[ |h_{S,2}[f]x_2[n, f]|^2 \right]}{E \left[ |h_{\Phi,1}[f]\sqrt{\Omega_{I,1}/\alpha_{\Phi,1}}x_1[n, f] + w_1[n, f]|^2 \right]} = \frac{\Omega_{S,2}E_{S,2}}{\frac{\Omega_{I,1}E_{S,1}}{\alpha_{\Phi,1}} + N_0} = \frac{1}{\frac{1}{\alpha_{\Phi,1}\text{SIR}_{\text{AS},1}} + \frac{1}{\text{SNR}_1}} \quad (8)$$

where  $N_0 = E[|w_1[n, f]|^2]$ ,  $\text{SNR}_1$  is the average received Signal to Noise Ratio (SNR) per symbol at Node 1, and  $\text{SIR}_{\text{AS},1}$  is the average received Signal to Interference Ratio (SIR) per symbol at Node 1 with only antenna separation and before applying any active cancellation. Hence,  $\text{SNR}_1 = \Omega_{S,2}E_{S,2}/N_0$ ,  $\text{SIR}_{\text{AS},1} = (\Omega_{S,2}E_{S,2})/(\Omega_{I,1}E_{S,1})$ , and using active self-interference cancellation mechanism  $\Phi$  improves the SIR by a factor of  $\alpha_{\Phi,1}$  compared to the SIR after antenna separation and before applying active cancellation.

To derive equations for Node 2 one can simply swap subindices 1 and 2 in all the equations we have derived so far to obtain

$$y_{\Phi,2}[n, f] = h_{S,1}[f]x_1[n, f] + h_{\Phi,2}[f]\sqrt{\Omega_{I,2}/\alpha_{\Phi,2}}x_2[n, f] + w_2[n, f], \quad (9)$$

and the average received SINR per symbol at Node 2 is equal to  $\text{SINR}_{\Phi,2} = 1/(\frac{1}{\alpha_{\Phi,2}\text{SIR}_{\text{AS},2}} + \frac{1}{\text{SNR}_2})$ , where  $\text{SNR}_2 = \Omega_{S,1}E_{S,1}/N_0$ ,  $\text{SIR}_{\text{AS},2} = (\Omega_{S,1}E_{S,1})/(\Omega_{I,2}E_{S,2})$ , and  $E[|w_2[n, f]|^2] = N_0$ .

From (7) and (9) we observe that the self interference at Node  $i$  depends on  $h_{\Phi,i}[f]$ ,  $\Omega_{I,i}$ ,  $\alpha_{\Phi,i}$ , and  $x_i[n, f]$ . We are interested in characterizing  $h_{\Phi,i}[f]$ ,  $\Omega_{I,i}$ , and  $\alpha_{\Phi,i}$  and analyzing their effect on full-duplex system performance.  $\Omega_{I,i}$  depends on the antenna directionality and the propagation loss of the signal traveling through wireless channel  $h_{I,i}[f]$ . Characterization of  $\Omega_{I,i}$  for different types of antennas and distances between same node antennas has been presented in [1, 2, 7], hence we will not present a characterization of  $\Omega_{I,i}$ . Characterization of  $h_{\Phi,i}[f]$  and  $\alpha_{\Phi,i}$  will be presented in Section IV and an analysis of achievable rate performance of full-duplex systems will be presented in Section V.

### III. EXPERIMENT SETUP AND SCENARIOS CONSIDERED

We used the WARPLab framework [8] to implement the experiment setup shown in Fig. 1. Two WARP nodes corresponding to Nodes 1 and 2 were connected via an Ethernet switch to

a host PC running MATLAB. The digital baseband waveforms (samples) that are input to the DACs at Node 1 and Node 2 were constructed in MATLAB and downloaded from the MATLAB workspace to transmit buffers in the FPGA of Node 1 and Node 2 respectively. Transmission and reception of over-the-air signals was done in real-time using the WARP hardware. The samples at the output of the ADC were stored in receiver buffers and loaded to the MATLAB workspace on the host PC and processing of these samples was done in MATLAB.

We now explain in more detail the way in which  $\hat{\kappa}_{AC,i}[f]$  for Node  $i = 1, 2$  was computed in our full-duplex implementation. We observed from experiment data that channels  $h_{1,i}[f]$  and  $h_{Z,i}[f]$  varied very slowly from one frame to the next. This slow variation was expected since channel  $h_{Z,i}[f]$  is a wire channel and channel  $h_{1,i}[f]$  is the wireless channel between two antennas that are fixed and at a small distance  $d$  from each other. Consequently, the computation of  $\hat{\kappa}_{AC,i}[f]$  in our full-duplex implementation took advantage of the slow variation of  $h_{1,i}[f]$  and  $h_{Z,i}[f]$  by averaging their ten most recent estimates. Specifically, in our experiments  $\hat{\kappa}_{AC,i}[f]$  was computed as  $\hat{\kappa}_{AC,i}[f] = \frac{\sum_{l=0}^L \frac{1}{L} \hat{h}_{1,i}[f-l]}{\sum_{l=0}^L \frac{1}{L} \hat{h}_{Z,i}[f-l]}$  where  $L = 10$ ,  $\hat{h}_{1,i}[f]$  denotes the noisy estimate of  $h_{1,i}[f]$ , and  $\hat{h}_{Z,i}[f]$  denotes the noisy estimate of  $h_{Z,i}[f]$ . Estimates  $\hat{h}_{1,i}[f]$  and  $\hat{h}_{Z,i}[f]$  were computed using training sent in every frame. We did experiments where we observed that computation of  $\hat{\kappa}_{AC,i}[f]$  using  $L = 10$  resulted in larger average amount of cancellation compared to using only  $L = 1$ . We also performed experiments where we observed that increasing  $L$  from 10 to 15 did not result in a measurable improvement of the average amount of cancellation achieved by analog cancellation. Hence, we decided to set  $L = 10$ . Characterizing the coherence time of the self-interference channel  $h_{1,i}[f]$  and the effect of different channel estimators on the amount of cancellation achieved by analog cancellation is important for the design of optimal training for computation of the cancellation coefficient. This is left as part of future work and for this paper the computation of  $\hat{\kappa}_{AC,i}[f]$  is based on averaging  $\hat{h}_{1,i}[f]$  and  $\hat{h}_{Z,i}[f]$  over ten frames as explained above.

In our full-duplex implementation the cancellation coefficient used for digital cancellation at Node  $i$  during frame  $f$  is equal to  $\hat{\kappa}_{DC,i}[f] = \hat{h}_{AC,i}[f]$  where  $\hat{h}_{AC,i}[f]$  denotes the noisy estimate of  $\tilde{h}_{AC,i}[f]$  which is computed every frame based on training. For computation of  $\hat{\kappa}_{DC,i}[f]$  we use only the most recent estimate of  $\tilde{h}_{AC,i}[f]$  because the value of  $\tilde{h}_{AC,i}[f]$  depends on errors in the estimate of  $h_{1,i}[f]$  and  $h_{Z,i}[f]$  and these estimation errors vary randomly from one frame to the next.

In our experiments both nodes were located at a height of 2 meters above the floor with a Line-Of-Sight (LOS) between all antennas. The distance between nodes was fixed to  $D = 8.5$  m. For the separation between same-node antennas we used values of  $d \in \{10 \text{ cm}, 20 \text{ cm}, 40 \text{ cm}\}$ . The antennas used were 2.4 GHz 7 dBi Desktop Omni [9]. We used transmission power values of  $P_T \in \{0 \text{ dBm}, 5 \text{ dBm}, 10 \text{ dBm}, 15 \text{ dBm}\}$ . We ran the experiments in the laboratory of the Center for Multimedia Communication at Rice University, the laboratory is located in the second floor of Duncan Hall building. We ran the experiments during school holiday recess, hence, there were few people walking in the lab and our experiment setup corresponds to a low mobility scenario. The sampling frequency of ADCs and DACs was equal to 40 MHz and we implemented a single subcarrier narrowband system with bandwidth of 0.625 MHz (hence the number of samples per symbol was equal to 128). The carrier frequency was centered at 2.4 GHz. Symbols were shaped using a Squared Root Raised Cosine pulse shaping filter with roll-off factor equal to one.

For our experiments, the number of symbols per frame was equal to 100 ( $N_{\text{sym}} = 100$ ) and the number of frames transmitted in one experiment was equal to 800 ( $N_{\text{frames}} = 800$ ). The value of  $N_{\text{sym}}$  was limited to 100 due to the characteristics of the transmitted signal (128 samples per symbol and 3584 samples used for frame preamble) and the total number of samples that can be stored per WARPLab buffer ( $2^{14}$ ). Setting  $N_{\text{frames}} = 800$  allowed us to approximate that during an experiment the channels conditions remained approximately constant and variations were only due to small scale variations.

#### IV. MEASUREMENT-BASED CHARACTERIZATION OF CHANNEL PARAMETERS

##### A. Average Cancellation by Active Cancellations

In our experiments, we used measurements of signal power before and after active cancellation in order to estimate  $\alpha_{\text{AC},i}$  and  $\alpha_{\text{ACDC},i}$  for each Node  $i = 1, 2$  as follows. For a fixed inter-antenna distance  $d$  at a node, and transmit power  $P_T$ , we measured the power of the received self-interference signal at Node  $i$  during frame  $f$ , which we label as  $P_{\text{RI},i}[f]$ . This measured power is the power of the self-interference simply due to path loss from antenna separation and before applying active cancellation. We also measured the power of the self-interference signal after analog cancellation at Node  $i$  during frame  $f$ , which we label as  $P_{\text{AC},i}[f]$ , and the power of the self-interference signal after combined analog and digital cancellation at Node  $i$  during frame  $f$ , which we label as  $P_{\text{ACDC},i}[f]$ . Per frame measurements of signal power were used to obtain

estimates of average power by averaging over all frames. Specifically, the average power of the received self-interference signal was computed as  $P_{\text{RI},i} = \sum_{f=1}^{N_{\text{frames}}} P_{\text{RI},i}[f]$ , the average power of the self-interference signal after analog cancellation was computed as  $P_{\text{AC},i} = \sum_{f=1}^{N_{\text{frames}}} P_{\text{AC},i}[f]$ , and the average power of the self-interference signal after analog and digital cancellation was computed as  $P_{\text{ACDC},i} = \sum_{f=1}^{N_{\text{frames}}} P_{\text{ACDC},i}[f]$ . Using these average powers we computed the value of  $\alpha_{\Phi}$ , for  $\Phi \in \{\text{AC}, \text{ACDC}\}$ , at Node  $i$  as  $\alpha_{\Phi,i} \text{ (dB)} = P_{\text{RI},i} \text{ (dBm)} - P_{\Phi,i} \text{ (dBm)}$ . The values of  $\alpha_{\text{AC},i}$  and  $\alpha_{\text{ACDC},i}$  from experimental data are shown in Figs. 2 and 3, respectively, as a function of  $P_{\text{RI},i}$ . In Figs. 2 and 3 we do not specify the values of  $d$ ,  $P_{\text{T}}$ , and  $i$  in order to avoid cluttering the figures and also because we did not observe any particular dependence of  $\alpha_{\text{AC},i}$  or  $\alpha_{\text{ACDC},i}$  as a function of  $d$ ,  $P_{\text{T}}$ , or  $i$  alone. However, as we will explain,  $\alpha_{\text{AC},i}$  and  $\alpha_{\text{ACDC},i}$  do depend on the resulting  $P_{\text{RI},i}$ .

We first note that the experimental data looks rather scattered and does not show smooth behavior; this is typical of experimental results [10]. Yet, several important conclusions can be drawn from the data. To understand the dominant trends, we compute the *constant fit*,  $\alpha_{\Phi,i}^{\text{con}}$ , and *linear fit*,  $\alpha_{\Phi,i}^{\text{lin}}$ , to the experimental data as shown in Figs. 2 and 3. The equations for  $\alpha_{\text{AC},i}^{\text{lin}}$  and  $\alpha_{\text{ACDC},i}^{\text{lin}}$ , computed using a least squares fit, are shown in Table I.

The key observation is that the linear fit captures the behavior of  $\alpha$  as a function of received interference power better than the constant fit. For example, for values of  $P_{\text{RI},i}$  lower than -40 dBm the constant fit  $\alpha_{\Phi,i}^{\text{con}}$  tends to overestimate the values of  $\alpha_{\Phi,i}$  and for values of  $P_{\text{RI},i}$  larger than -25 dBm the constant fit  $\alpha_{\Phi,i}^{\text{con}}$  tends to underestimate the value of  $\alpha_{\Phi,i}$ . The better fit between the experiment data and the linear fit leads to the following first result.

*Result 1:* As the average power of the received self-interference,  $P_{\text{RI},i}$ , increases, the average amount of interference suppression achieved by active cancellation (both AC and ACDC) also increases.

*Reasons for Result 1:* In order to implement the active cancellation mechanisms, we first need to estimate the wireless self-interference channel. The average power of the signal used to estimate the wireless self-interference channel is  $P_{\text{RI},i}$ . As  $P_{\text{RI},i}$  increases, the noise in the estimation of the wireless self-interference channel decreases, and thus, the cancellation process is more exact leading to larger suppression of self-interference. ■

Result 1 captures the total average performance of self-interference cancellation for both  $\Phi = \{\text{AC}, \text{ACDC}\}$ . We dig deeper into the relative contributions of analog and digital cancellation

in ACDC and discover the following result.

*Result 2:* As the average performance of analog cancellation gets better, the average effectiveness of digital cancellation after analog cancellation reduces.

In Fig. 4, we plot the average amount of cancellation achieved by digital cancellation after analog cancellation, computed as  $\alpha_{\text{DC},i}$  (dB) =  $\alpha_{\text{ACDC},i}$  (dB) -  $\alpha_{\text{AC},i}$  (dB), as a function of the average amount of cancellation achieved by analog cancellation. Results in Fig. 4 show that, in agreement with Result 2, as  $\alpha_{\text{AC},i}$  increases  $\alpha_{\text{DC},i}$  decreases.

In Fig. 4 we also show the value of  $\alpha_{\text{DC},i}$  computed based on the constant fit and the linear fit. For the constant fit  $\alpha_{\text{DC},i}^{\text{con}}$  (dB) =  $\alpha_{\text{ACDC},i}^{\text{con}}$  -  $\alpha_{\text{AC},i}^{\text{con}}$  = 1.1 (dB). For the linear fit, we use the equations for  $\alpha_{\text{AC},i}^{\text{lin}}$  and  $\alpha_{\text{ACDC},i}^{\text{lin}}$  to compute  $\alpha_{\text{DC},i}^{\text{lin}}$  (dB) =  $\alpha_{\text{ACDC},i}^{\text{lin}}$  (dB) -  $\alpha_{\text{AC},i}^{\text{lin}}$  (dB) =  $\lambda_{\text{ACDC}}(\alpha_{\text{AC},i}^{\text{lin}}$  (dB) -  $\beta_{\text{AC}})/\lambda_{\text{AC}}$  +  $\beta_{\text{ACDC}}$  -  $\alpha_{\text{AC},i}^{\text{lin}}$  (dB). Results in Fig. 4 show that the dominant behavior is again better captured by the linear fit.

Dual to Result 2 is the following result.

*Result 3:* The smaller the amount of suppression achieved by analog cancellation during a frame, the larger the probability that applying digital cancellation after analog cancellation will result in an increase of the total suppression during that frame.

In contrast to the average system performance in Results 1 and 2, Result 3 relates to frame-by-frame performance. In our experiments, the suppression achieved by analog cancellation during frame  $f$  was computed as  $\alpha_{\text{AC},i}[f]$  (dB) =  $\text{P}_{\text{RI},i}[f]$  (dBm) -  $\text{P}_{\text{AC},i}[f]$  (dBm) and the suppression achieved by analog and digital cancellation during frame  $f$  was computed as  $\alpha_{\text{ACDC},i}[f]$  (dB) =  $\text{P}_{\text{RI},i}[f]$  (dBm) -  $\text{P}_{\text{ACDC},i}[f]$  (dBm). The suppression achieved by digital cancellation after analog cancellation during frame  $f$  was computed as  $\alpha_{\text{DC},i}[f] = \alpha_{\text{ACDC},i}[f] - \alpha_{\text{AC},i}[f]$ . Digital cancellation resulted in an increase in total suppression during frame  $f$  if  $\alpha_{\text{DC},i}[f]$  (dB) > 0.

Result 3 is verified by results in Fig. 5 which show the probability that digital cancellation results in an increase in total suppression during a frame as a function of the suppression achieved by analog cancellation during a frame. For example, for values  $\alpha_{\text{AC},i}[f]$  between 24 dB and 25 dB the probability of having  $\alpha_{\text{DC},i}[f]$  (dB) > 0 is equal to 95 %. Results shown in Fig. 5 were computed based on experiment data. We observe from Fig. 5 that digital cancellation after analog cancellation becomes more effective as  $\alpha_{\text{AC},i}[f]$  decreases. Fig. 5 shows that digital cancellation is effective for the frames where analog cancellation achieves less than 32 dB of suppression, since in these frames the probability that digital cancellation increases the total suppression is

greater than 50 %. However, for frames where analog cancellation achieves more than 32 dB of cancellation, applying digital cancellation after analog cancellation is not effective since the probability that digital cancellation results in an increase of the total amount of cancellation is less than 50 % hence it is most likely that digital cancellation will increase the self-interference. Based on Result 3 we propose a design rule for full duplex systems which will be presented in Section V-C.

*Reasons for Result 2 and Result 3:* Intuitively it is clear that if analog cancellation can achieve perfect cancellation (infinite dB of cancellation) then digital cancellation is unnecessary. In fact, if analog cancellation can achieve perfect cancellation then applying digital cancellation can result in an increase in the self-interference. This can be observed from (2). Notice that in case of perfect analog cancellation we have that  $\tilde{h}_{AC,1}[f] = 0$  but due to noise in the system the value of  $\hat{\kappa}_{DC,1}[f]$  will not be equal to zero and will correspond to a measurement of noise hence adding  $-\hat{\kappa}_{DC,1}[f]x_1[n, f]$  to the signal after analog cancellation will result in an increase in the self-interference. We observe that as the performance of analog cancellation improves, the noise in the estimation of  $\tilde{h}_{AC,i}[f]$  increases since  $\tilde{h}_{AC,i}[f]$  becomes a smaller quantity and this reduces the effectiveness of applying digital cancellation after analog cancellation. Although our implementation of analog cancellation does not achieve perfect cancellation we do observe from experiment results in Fig. 5 that for values of  $\alpha_{AC,i}[f]$  larger than 32 dB it is most likely that applying digital cancellation will increase the self-interference. This is consistent with average performance results in Fig. 4 which show that when the average cancellation achieved by analog cancellation is larger than 30 dB then digital cancellation after analog cancellation can result in an increase the average self-interference which results in negative values of  $\alpha_{DC,i}$ . ■

All the active cancellation schemes that we have considered are a linear function of the self-interference. For example, we use  $-\hat{\kappa}_{AC,1}[f]x_{RF,1}(t)$  for analog cancellation and  $-\hat{\kappa}_{DC,1}[f]x_1[n, f]$  for digital cancellation at Node 1. Notice from Fig. 2 and 3 that the values of  $\alpha_{AC,i}$  and  $\alpha_{ACDC,i}$  obtained from experiments were never larger than 36 dB. Other implementations of active cancellation mechanisms that are a linear function of the self-interference signal have reported no more than 37 dB of cancellation [3, 11] and 30 dB of cancellation for the cancellation implementation in [1]. To achieve more than 37 dB of average cancellation, nonlinear schemes for active cancellation may be needed.

### B. Characterizing the $K$ -factor

We assume that the magnitude of the self-interference channel before active cancellation and the magnitude of the self-interference channel after active cancellation have a Ricean distribution. Intuitively the Ricean assumption makes sense because before applying active cancellation the self-interference channel is the channel between two antennas that are close to each other. Hence there is a strong LOS component and the effect of active cancellation would be a reduction of the LOS component [5]. Also, we have done a comparison between histograms of channel estimate magnitudes obtained from experiments and the probability density function of a Ricean distribution and we have observed a good fit. Thus, all evidence supports the conclusion that Ricean is a good model for the magnitude of the self-interference channel. Hence, we model  $|h_{I,i}[f]|$  and  $|h_{\Phi,i}[f]|$  as Ricean distributions with  $K$ -factor  $K_{I,i}$  and  $K_{\Phi,i}$  respectively. In this section we present a characterization of  $K_{I,i}$  and  $K_{\Phi,i}$  based on experiments.

Estimates of  $K_{I,i}$  and  $K_{\Phi,i}$  were computed based on experiment data and the moment based estimator presented in Equation (3) of [12]. Each value of  $K_{I,i}$ ,  $K_{\Phi,i}$  that we computed was based on 800 consecutive measurements of  $|h_{I,i}[f]|$  and  $|h_{\Phi,i}[f]|$  respectively made at a fixed  $d$ , and  $P_T$ . We note that the variations in each set of 800 consecutive measurements corresponded to small scale variations hence each set of 800 measurements can be used to obtain one estimate of the  $K$ -factor.

We first characterize the self-interference channel before active cancellation. We aggregate  $K_{I,i}$  values computed for  $i = 1, 2$  and different values of  $P_T$  to obtain the CDF of  $K_{I,i}$  for a fixed  $d$ . Fig. 6 shows the CDF of  $K_{I,i}$  computed for  $d = 10$  cm, the CDF of  $K_{I,i}$  computed for  $d = 20$  cm, and the CDF of  $K_{I,i}$  computed for  $d = 40$  cm. Each of these three CDFs is the result of a total of 16 independent estimates of  $K_{I,i}$  at a fixed  $d$ .

Results in Fig. 6 show that the value of  $K_{I,i}$  for  $d$  between 10 cm and 40 cm is between 25 dB and 40 dB. These large values of  $K_{I,i}$  were expected due to the proximity of same node antennas. It is expected that as the distance between antennas increases the value of  $K_{I,i}$  decreases. Hence, the CDF of  $K_{I,i}$  for  $d = 40$  cm should be more to the left than the CDF of  $K_{I,i}$  for  $d = 20$  cm and the CDF  $K_{I,i}$  for  $d = 10$  cm should be more to the right. However, results in Fig. 6 do not show a clear difference between the CDFs for  $d = 10$  cm,  $d = 20$  cm and  $d = 40$  cm. Our intuition is that an increase in separation from  $d = 10$  cm to  $d = 40$  cm results in a decrease in

$K_{I,i}$  that is smaller than the error in our estimate, hence it is not captured by the CDFs shown in Fig. 6. To support this intuition we also show in Fig. 6 the CDF of  $K_{S,i}$  which is the estimate of the  $K$ -factor of the distribution of  $|h_{S,i}[f]|$ . Since  $h_{S,i}[f]$  is the channel between two antennas at LOS placed at distance  $D = 8.5$  m the CDF of  $K_{S,i}$  should be noticeably to the left of the CDF of  $K_{I,i}$  and this is verified by results in Fig. 6.

Next, we characterize  $K$ -factor of the self-interference channel after active cancellation and verify the following result.

*Result 4:* The  $K$ -factor for the self-interference channel reduces due to active cancellation and the amount of reduction increases as the self-interference suppression increases. Hence, the  $K$ -factor for the self-interference channel after active cancellation depends on the  $K$ -factor value before active cancellation and the suppression achieved by active cancellation.

The CDF of  $K_{AC,i}$  and the CDF of  $K_{ACDC,i}$  are shown in Fig. 6. We obtained the CDF of  $K_{AC,i}$  and  $K_{ACDC,i}$  by aggregating the  $K$ -factors estimated at Nodes 1 and 2 for different values of  $d$  and  $P_T$ . Results in Fig. 6 show that the  $K$ -factor before active cancellation is larger than the  $K$ -factor after active cancellation. Hence, the  $K$ -factor for the self-interference channel reduces due to active cancellation. This reduction in  $K$ -factor is a function of the suppression achieved by active cancellation. This is verified by experiment results shown in Fig. 7 where we plot the reduction in  $K$ -factor due to active cancellation mechanism  $\Phi$  (this reduction is computed as  $K_{I,i}$  (dB)  $-$   $K_{\Phi,i}$  (dB)) as a function of the average amount of suppression  $\alpha_{\Phi,i}$  for  $\Phi \in \{AC, ACDC\}$ . As the suppression increases, the reduction in  $K$ -factor also increases.

*Reasons for Result 4:* Active cancellation is based on estimation of the self-interference channel. Before active cancellation the self-interference channel has a strong LOS component, hence, an estimate of the self-interference channel before active cancellation is virtually an estimate of the strong LOS component of this channel. Consequently, most of the cancellation applied by active cancellation corresponds to attenuation of the strong LOS component that is present before active cancellation and as the suppression achieved by active cancellation increases the attenuation of the LOS component also increases. ■

## V. ACHIEVABLE RATES

### A. Computation of Achievable Rates

We compute the achievable rate based on the SINR per frame which is estimated based on the Average Error Vector Magnitude Squared (AEVMS) [13] per frame. The AEVMS per frame transmitted to Node  $i$  is estimated as follows. Symbol  $s_i[n, f]$  is sent to Node  $i$  and Node  $i$  computes an estimate of  $s_i[n, f]$  which we label as  $\hat{s}_i[n, f]$ . The AEVMS per frame transmitted to Node  $i$  is estimated as  $\text{AEVMS}_i[f] = \frac{1}{N_{\text{sym}}} \sum_{n=1}^{N_{\text{sym}}} |s_i[n, f] - \hat{s}_i[n, f]|^2$ . The SINR for frame  $f$  received at Node  $i$  is estimated as  $\text{SINR}_i[f] = 1/\text{AEVMS}_i[f]$  and the achievable rate for frame  $f$  received at Node  $i$  is estimated as  $\text{AR}_i[f] = \log_2(1 + \text{SINR}_i[f])$ . The achievable sum rate of the full-duplex two-way system is computed by averaging over all the achievable sum rates per frame and it is equal to  $\text{ASR} = \frac{1}{N_{\text{frames}}} \sum_{f=1}^{N_{\text{frames}}} (\log_2(1 + \text{SINR}_1[f]) + \log_2(1 + \text{SINR}_2[f]))$ . The achievable rate for transmission to Node  $i$  is computed by averaging over all the achievable rates per frame and it is equal to  $\text{AR}_i = \frac{1}{N_{\text{frames}}} \sum_{f=1}^{N_{\text{frames}}} \log_2(1 + \text{SINR}_i[f])$ .

In our experiments we used symbols  $s_1[n, f]$  and  $s_2[n, f]$  that were modulated using QPSK. However, notice that the AEVMS value is independent of the constellation size and shape chosen for symbols  $s_1[n, f]$  and  $s_2[n, f]$ , this was also discussed in [13]. The numerator in the computation of  $\text{SINR}_i[f]$  is equal to one because we are using a normalized constellation, if the average energy per symbol was not equal to one then  $\text{SINR}_i[f]$  would have to be scaled by a normalization factor.

### B. Achievable Rates with Increasing Power

Our key result based on experimental data is as follows.

*Result 5:* If the Signal to Interference Ratio before active cancellation at Node  $i$ ,  $\text{SIR}_{\text{AS},i}$ , is maintained constant while the average received self-interference power at Node  $i$ ,  $\text{P}_{\text{RI},i}$ , is increased, then the achievable rate for transmission to Node  $i$  increases.

Experiment results that verify Result 5 are shown in Fig. 8. The solid line in Fig. 8 shows the achievable rates for transmission to Node 1 in a Full-Duplex system where nodes use Analog Cancellation (FD-AC) and no digital cancellation. The dashed line in Fig. 8 shows the achievable rates for transmission to Node 1 in a Full-Duplex system where nodes use Analog Cancellation and Digital Cancellation (FD-ACDC). Results for the full-duplex system with analog cancellation

and no digital cancellation correspond to an  $\text{SIR}_{\text{AS},1}$  value of approximately -20 dB. Results for the full-duplex system with analog cancellation and digital cancellation correspond to an  $\text{SIR}_{\text{AS},1}$  value of approximately -13 dB. For each full-duplex system considered in Fig. 8 we observe that although the value of  $\text{SIR}_{\text{AS},1}$  is approximately constant, the achievable rate at Node 1 is increasing as  $P_{\text{RI},1}$  increases.

*Reasons for Result 5:* Result 5 can be explained using our derived equations and Result 1 as follows. In Result 1 of Section IV-A we showed that  $\alpha_{\Phi,i}$  increases as  $P_{\text{RI},i}$  increases. In Section II-E we obtained that the SINR at Node  $i$  when using active self-interference cancellation mechanism  $\Phi$  is given by  $\text{SINR}_{\Phi,i} = 1 / (\frac{1}{\alpha_{\Phi,i} \text{SIR}_{\text{AS}_i}} + \frac{1}{\text{SNR}_i})$ . The equation for  $\text{SIR}_{\text{AS}_i}$  can be written in terms of average received powers as  $\text{SIR}_{\text{AS}_i}$  (dB) =  $P_{\text{RS},i}$  (dBm) -  $P_{\text{RI},i}$  (dBm), where  $P_{\text{RS},i}$  is the average power of the signal of interest received at Node  $i$ . If  $\text{SIR}_{\text{AS}_i}$  remains constant while  $P_{\text{RI},i}$  increases then this means that  $P_{\text{RS},i}$  is increasing and the rate of increase of  $P_{\text{RS},i}$  is the same rate of increase as  $P_{\text{RI},i}$ . Hence, if  $\text{SIR}_{\text{AS}_i}$  remains constant while  $P_{\text{RI},i}$  increases then the terms in the equation for  $\text{SINR}_{\Phi,i}$  that are changing are  $\alpha_{\Phi,i}$  and  $\text{SNR}_i$  and they are both increasing consequently  $\text{SINR}_i$  increases and this results in an increase in achievable rate. ■

Notice that if the transmission power at Node 1 and Node 2 in Fig. 1 is increased by the same amount then  $\text{SIR}_{\text{AS},1}$  and  $\text{SIR}_{\text{AS},2}$  will not change and  $P_{\text{RI},1}$  and  $P_{\text{RI},2}$  will increase hence, as can be concluded from Result 5, the achievable rate in both directions of the link will increase. Hence, Result 5 leads to the following design rule for two-way full-duplex systems.

*Design Rule 1 (Rate-Power Increase):* In a two way full-duplex system like the one shown in Fig. 1 increasing the transmission power at both nodes by the same amount results in an increase of the achievable rate in both directions of the link and this increases the achievable sum rate of the full-duplex system.

Experiment and simulation results that verify our design rule are shown in Fig. 9. Results in Fig. 9 correspond to  $D = 8.5$  m and both nodes transmitting using the same power  $P_{\text{T}}$ . We show experiment results for a Full-Duplex system with Analog Cancellation and Digital Cancellation (FD-ACDC) with  $d = 10$  cm. We also show experiment results for a Full-Duplex system with Analog Cancellation and no digital Cancellation (FD-AC) with  $d = 20$  cm and  $d = 40$  cm and we show simulation results for the FD-AC system with  $d = 20$  cm. Simulation results shown in Fig. 9 were obtained using the equations for received signal in (7) and (9) and the equation parameters were set based on measurements made at Node 1 and Node 2 for  $d = 20$  cm. A

summary of the parameters used in simulation for each value of  $P_T$  is shown in Table II. Results in Fig. 9 show that the achievable sum rate increases as the transmission power increases and this verifies our design rule for full-duplex systems. For the experiment results shown in Fig. 9, we observed that the value of  $\frac{1}{\alpha_{\Phi,i}\text{SIR}_{AS_i}}$  was always between 20 dB to 45 dB larger than  $\frac{1}{\text{SNR}_i}$ . Thus, the performance of the full-duplex systems that we implemented was dominated by the self-interference and not by the additive noise. Hence, in our simulation we simplified  $w_1[f] = w_2[f] = 0$  since this noise term was not dominant and having a good estimate of  $N_0$  can be difficult [13]. Simulation results in Fig. 9 also serve to show that the equations we have derived and our characterization in Section IV do capture the dominant factors of performance.

### C. Achievable Rates with Selective Digital Cancellation

In Section IV we analyzed the performance of analog and digital cancellation. From results in Fig. 5 we observed that there are frames where applying digital cancellation after analog cancellation can reduce the self-interference but there are also frames where it can increase the self-interference. We would like to apply digital cancellation only during frames where it can help reduce the self-interference.

Notice that training signals can be used to estimate  $\alpha_{DC,i}[f]$ , which is the amount of cancellation achieved by digital cancellation after analog cancellation during frame  $f$  at Node  $i$ . Using  $\alpha_{DC,i}[f]$  estimated based on training, Node  $i$  can decide if digital cancellation should be applied to frame  $f$  based on the following design rule.

*Design Rule 2 (Selective Digital Cancellation):* If  $\alpha_{DC,i}[f] > 0$  then apply digital cancellation to the payload received at Node  $i$  during frame  $f$ , otherwise do not apply digital cancellation to the payload received at Node  $i$  during frame  $f$ .

We performed experiments for a full-duplex system with analog cancellation and the frames received were stored and post-processed in the following three different ways. (1) We did not apply digital cancellation to the received payload and this payload was used to compute the achievable sum rate of a Full-Duplex system with Analog Cancellation (FD-AC). (2) We applied digital cancellation to the received payload of all frames and the resulting payload was used to compute the achievable sum rate of a Full-Duplex system with Analog Cancellation and Digital Cancellation (FD-ACDC). (3) We applied digital cancellation to the received payload selectively based on Design Rule 2 and the resulting payload was used to compute the achievable sum rate of

a Full-Duplex system with Analog Cancellation and Selective Digital Cancellation (FD-ACSDC) based on Design Rule 2. Fig. 10 shows achievable sum rate results for these three full-duplex systems. Results in Fig. 10 correspond to  $d = 20$  cm and  $D = 8.5$  m. The transmission power at Node 1 and Node 2 was equal to  $P_T$ . Each thick bar in Fig. 10 shows the achievable sum rate averaged over all frames. The lower end of each thin bar in Fig. 10 indicates the lowest achievable sum rate per frame obtained for the corresponding full-duplex system and the upper end of each thin bar indicates the largest achievable sum rate per frame obtained for the corresponding full duplex system. Hence, thin bars show the range of achievable sum rate values observed for each full-duplex system and thick bars show the average over all the achievable sum rate values per frame.

By comparing the thick bars in Fig. 10, we conclude that the best full-duplex system is the one that applies digital cancellation selectively based on Design Rule 2. By comparing the lower end of the thin bars in Fig. 10, we observe that the lowest achievable sum rate per frame was always higher for the systems that use digital cancellation. The reason is that for the frames where analog cancellation has poor performance (leading to a low achievable sum rate of the FD-AC system for those frames) digital cancellation can increase the total self-interference suppression and this leads to a larger achievable sum rate for the FD-ACDC and FD-ACSDC systems for those frames. Hence, digital cancellation is an excellent *safety net* for the frames where analog cancellation delivers poor suppression. A comparison of the upper end of the thin bars in Fig. 10 shows that applying digital cancellation all the time can sometimes result in a reduction of the achievable sum rate but applying digital cancellation selectively based on Design Criteria 2 avoids applying digital cancellation in frames where it would result in a decrease in achievable sum rate.

## VI. CONCLUSIONS

We presented an experiment based characterization of analog and digital self-interference cancellation mechanisms. Using our theoretical framework and our experiments results, we analyzed how different active cancellation mechanisms affect the performance of full-duplex two-way wireless communication systems. Our results illustrate the factors that dominate the performance of full-duplex two-way wireless communications and lead to design rules for the implementation of these systems.

## REFERENCES

- [1] J. I. Choi, M. Jain, K. Srinivasan, P. Levis, and S. Katti, "Achieving single channel, full duplex wireless communication," in *MobiCom*, 2010.
- [2] M. Duarte and A. Sabharwal, "Full-duplex wireless communications using off-the-shelf radios: Feasibility and first results," in *Asilomar Conference on Signals, Systems, and Computers*, 2010.
- [3] S. Chen, M. Beach, and J. McGeehan, "Division-free duplex for wireless applications," in *IEEE Electronics Letters*, vol. 34, no. 2, 1998, pp. 147–148.
- [4] B. Radunovic, D. Gunawardena, P. Key, A. P. N. Singh, V. Balan, and G. Dejean, "Rethinking indoor wireless: Low power, low frequency, full duplex," Microsoft Research, Tech. Rep. MSR-TR-2009-148, 2009.
- [5] H. Ju, S. Lee, K. Kwak, E. Oh, and D. Hong, "A new duplex without loss of data rate and utilizing selection diversity," in *IEEE Vehicular Technology Conference*, 2008.
- [6] "Rice university WARP project." [Online]. Available: <http://warp.rice.edu>
- [7] K. Haneda, E. Kahra, S. Wyne, C. Icheln, and P. Vainikainen, "Measurement of loop-back interference channels for outdoor-to-indoor full-duplex radio relays," in *Proceedings of the fourth European Conference on Antennas and Propagation EUCAP*, 2010.
- [8] "WARPLab framework." [Online]. Available: <http://warp.rice.edu/trac/wiki/WARPLab>
- [9] "RE07U-SM." [Online]. Available: <http://www.l-com.com/item.aspx?id=21447>
- [10] T. S. Rappaport, *Wireless Communications: Principles and Practice*, 2nd ed. Prentice Hall, 2001.
- [11] W. Schacherbauer, A. Springer, T. Ostertag, C. Ruppel, and R. Weigel, "A flexible multiband frontend for software radios using high if and active interference cancellation," in *IEEE International Microwave Symposium*, 2001.
- [12] A. Abdi, C. Tepedelenlioglu, M. Kaveh, and G. Giannakis, "On the estimation of the K parameter for the rice fading distribution," *IEEE Communications Letters*, vol. 5, no. 3, pp. 92–94, March 2001.
- [13] M. Duarte, A. Sabharwal, C. Dick, and R. Rao, "Beamforming in MISO systems: Empirical results and EVM-based analysis," *IEEE Trans. Wireless Comm.*, vol. 9, no. 10, pp. 3214–1276, October 2010.

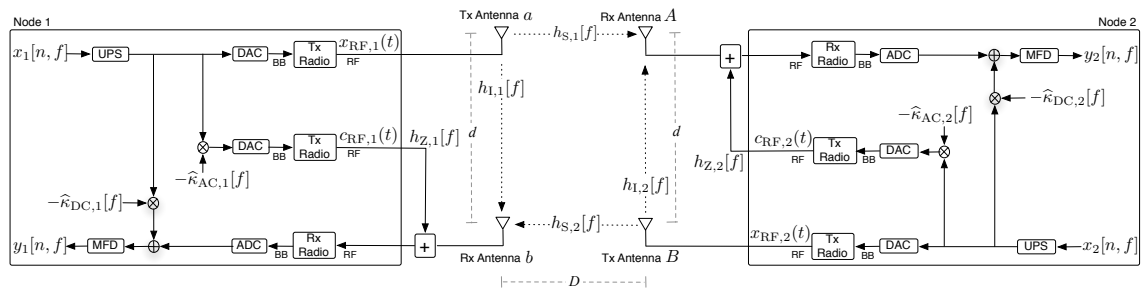


Fig. 1. Block diagram of a full-duplex system.

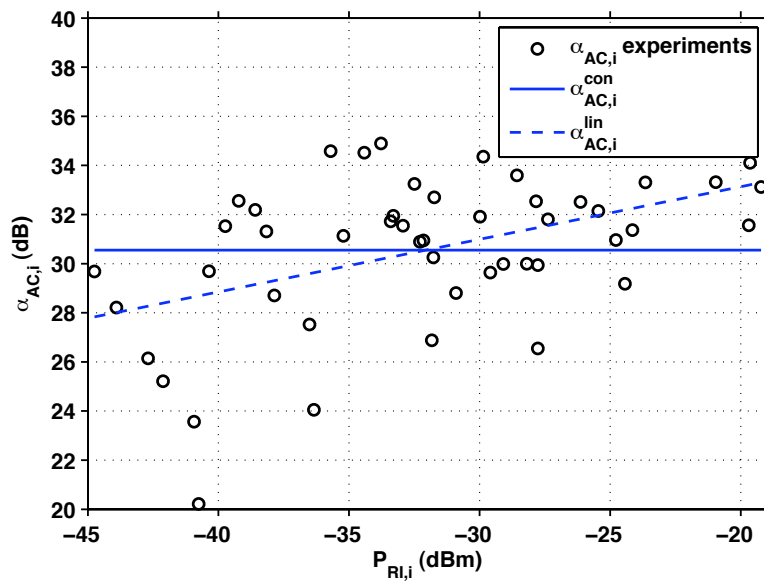


Fig. 2. Measurements of the average amount of cancellation achieved by analog cancellation and constant and linear fit for the measurements.

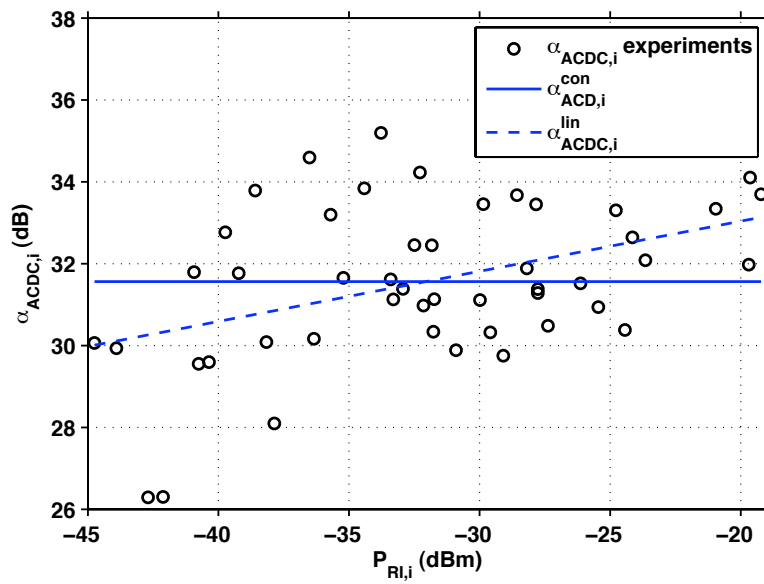


Fig. 3. Measurements of the average amount of cancellation achieved by combined analog and digital cancellation and constant and linear fit for the measurements.

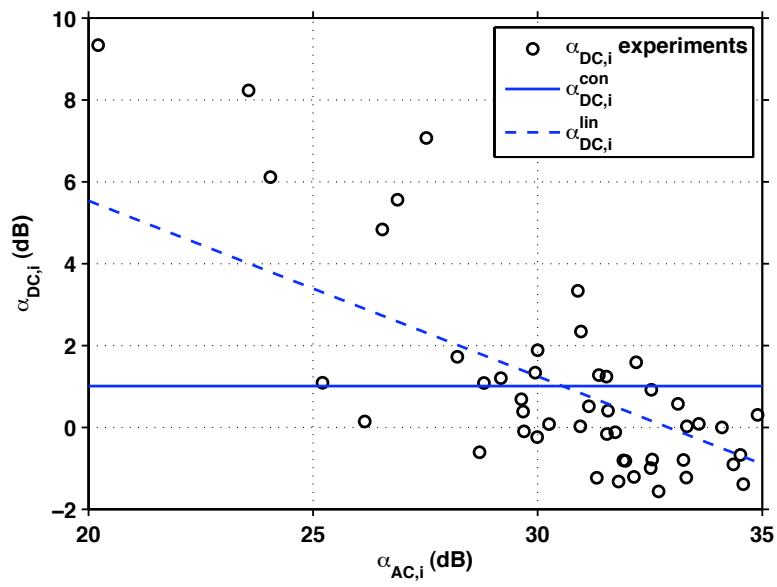


Fig. 4. Measurements of the average amount of cancellation achieved by digital cancellation and cancellation values computed based on the constant and linear fit.

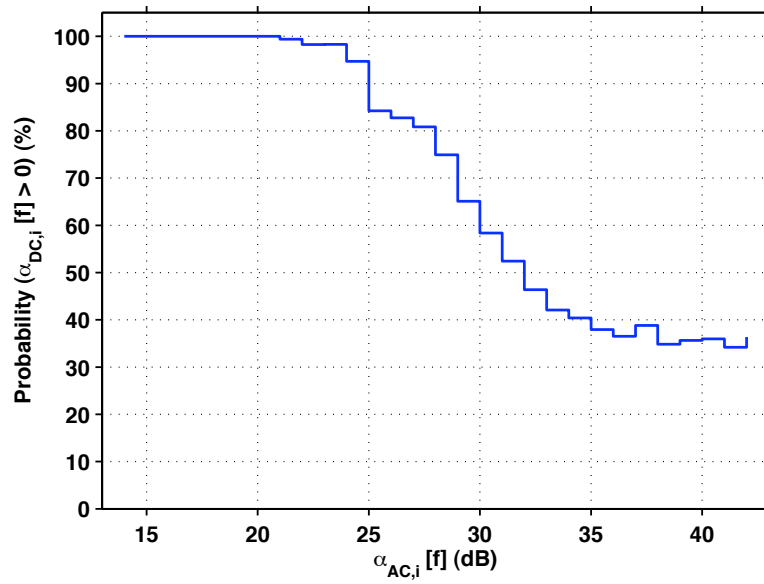


Fig. 5. Probability that digital cancellation after analog cancellation increases the total amount of cancellation during a frame as a function the cancellation achieved by analog cancellation

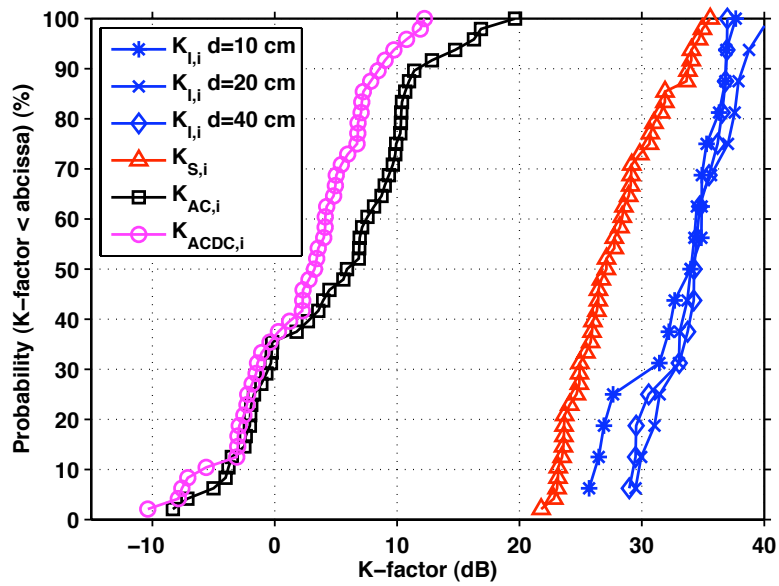


Fig. 6. CDF of  $K$ -factor.

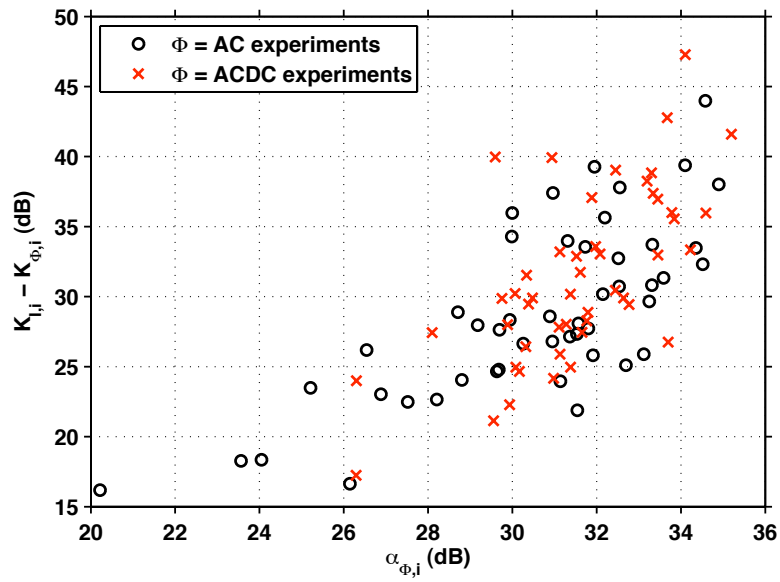


Fig. 7. Reduction in  $K$ -factor as a function of the average amount of cancellation.

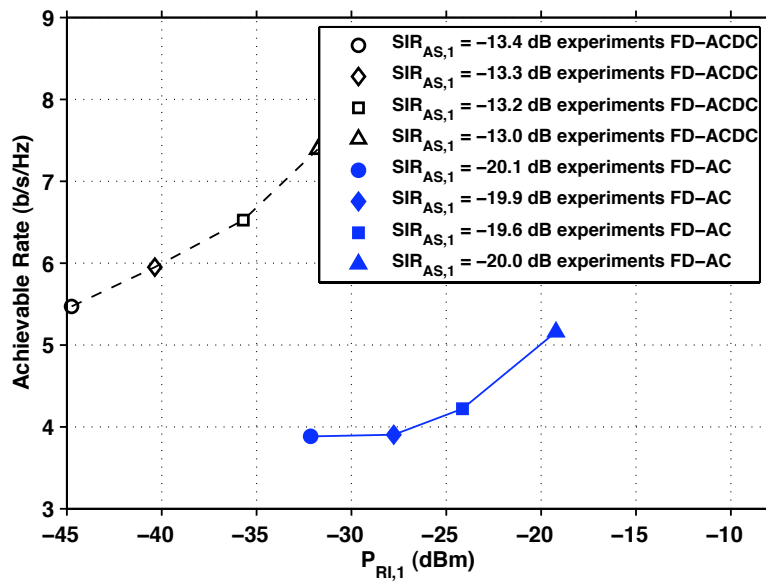


Fig. 8. Experiment results showing the achievable rate at Node 1 as a function of the average received self-interference power for an approximately constant value of  $SIR_{AS,1}$ .

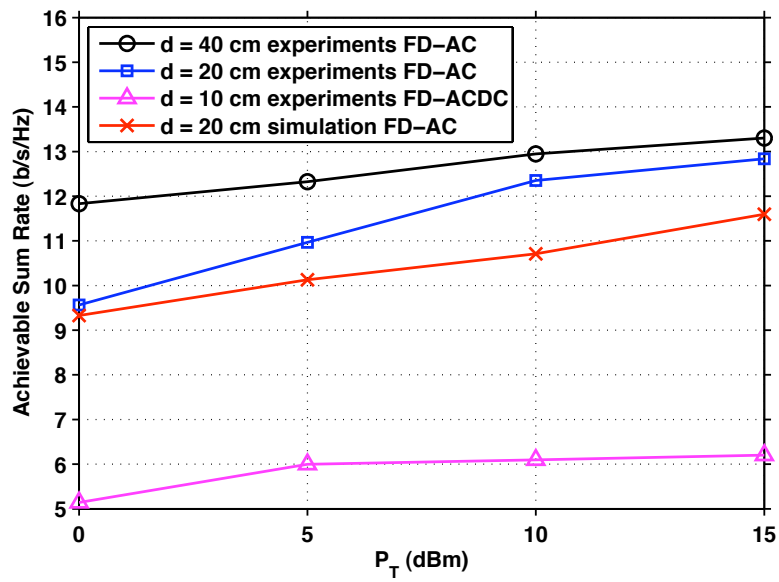


Fig. 9. Experiment and simulation results showing an increase in the achievable sum rate as a function of the transmission power for a full-duplex two-way system using the same transmission power at both nodes.

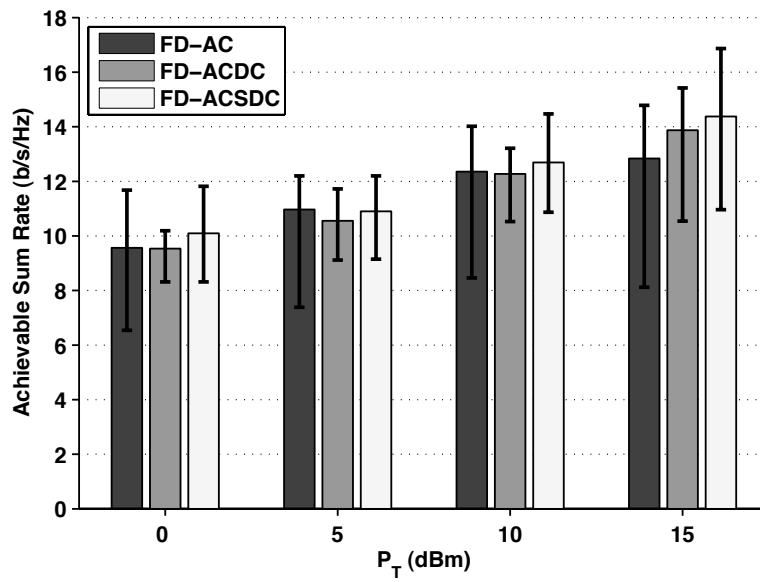


Fig. 10. Experiment results showing the effect of different cancellation schemes on the achievable sum rate of a full-duplex two-way system using the same transmission power at both nodes.

**TABLE I**  
**CONSTANT AND LINEAR FIT FOR MEASURED VALUES OF AVERAGE CANCELLATION**

| Parameter  | Constant Fit                                      | Linear fit  |
|--|---|---|
| Average cancellation achieved by analog cancellation at Node $i$             | $\alpha_{AC,i}^{\text{con}} = 30.55 \text{ dB}$   | $\alpha_{AC,i}^{\text{lin}} = \lambda_{AC} P_{\text{RI},i} + \beta_{AC}$ where<br>$\lambda_{AC} = 0.21 \text{ dB/dBm}$ and<br>$\beta_{AC} = 37.42 \text{ dB}$           |
| Average cancellation achieved by analog and digital cancellation at Node $i$ | $\alpha_{ACDC,i}^{\text{con}} = 31.56 \text{ dB}$ | $\alpha_{ACDC,i}^{\text{lin}} = \lambda_{ACDC} P_{\text{RI},i} + \beta_{ACDC}$<br>where $\lambda_{ACDC} = 0.12 \text{ dB/dBm}$ and<br>$\beta_{ACDC} = 35.49 \text{ dB}$ |

TABLE II  
SIMULATION PARAMETERS BASED ON MEASUREMENTS AT NODE 1 AND NODE 2 FOR  $d = 20$  CM.

| Parameter            | $P_T$                 |                       |                       |                       |
|----------------------|-----------------------|-----------------------|-----------------------|-----------------------|
|                      | 0 dBm                 | 5 dBm                 | 10 dBm                | 15 dBm                |
| $SIR_{AS,1}$ (dB)    | -18.5                 | -18.8                 | -18.7                 | -17.8                 |
| $SIR_{AS,2}$ (dB)    | -12.5                 | -11.6                 | -11.8                 | -11.7                 |
| $P_{RI,1}$ (dBm)     | -39.2                 | -34.4                 | -29.9                 | -26.1                 |
| $P_{RI,2}$ (dBm)     | -40.8                 | -36.3                 | -31.8                 | -27.8                 |
| $K_{AC,1}$ (dB)      | 15.3                  | 12.8                  | 10.2                  | 9.1                   |
| $K_{AC,2}$ (dB)      | 15.3                  | 12.8                  | 10.2                  | 9.1                   |
| $K_{S,1}$ (dB)       | 29.5                  | 29.5                  | 29.5                  | 29.5                  |
| $K_{S,2}$ (dB)       | 29.5                  | 29.5                  | 29.5                  | 29.5                  |
| $N_0$ (dBm)          | $\infty$              | $\infty$              | $\infty$              | $\infty$              |
| $\alpha_{AC,1}$ (dB) | $\alpha_{AC,1}^{lin}$ | $\alpha_{AC,1}^{lin}$ | $\alpha_{AC,1}^{lin}$ | $\alpha_{AC,1}^{lin}$ |
| $\alpha_{AC,2}$ (dB) | $\alpha_{AC,2}^{lin}$ | $\alpha_{AC,2}^{lin}$ | $\alpha_{AC,2}^{lin}$ | $\alpha_{AC,2}^{lin}$ |